ADVANCES IN ATMOSPHERIC SCIENCES, VOL. 27, NO. 5, 2010, 1131–1142

An Introduction to the Coupled Model FGOALS1.1-s and Its Performance in East Asia

BAO Qing*[1] (包 庆), WU Guoxiong[1] (吴国雄), LIU Yimin[1] (刘屹岷), YANG Jing[2] (杨 静), WANG Zaizhi[3] (王在志), and ZHOU Tianjun[1] (周天军)

[1]*State Key Laboratory of Numerical Modeling for Atmospheric Sciences and Geophysical Fluid Dynamics, Institute of Atmospheric Physics, Chinese Academy of Sciences, Beijing* 100029

[2]*ESPRE, Beijing Normal University, Beijing* 100875

[3]*Beijing Climate Center, China Meteorological Administration, Beijing* 100081

(Received 21 October 2009; revised 13 December 2009)

ABSTRACT

The spectral version 1.1 of the Flexible Global Ocean–atmosphere–land System (FGOALS1.1-s) model was developed in the State Key Laboratory of Numerical Modeling for Atmospheric Sciences and Geophysical Fluid Dynamics at the Institute of Atmospheric Physics (LASG/IAP). This paper reports the major modifications to the physical parameterization package in its atmospheric component, including the radiation scheme, convection scheme, and cloud scheme. Furthermore, the simulation of the East Asian Summer Monsoon (EASM) by FGOALS1.1-s is examined, both in terms of climatological mean state and interannual variability.

The results indicate that FGOALS1.1-s exhibits significant improvements in the simulation of the balance of energy at the top of the atmosphere: the net radiative energy flux at the top was 0.003 W m^{-2} in the 40 years fully coupled integration. The distribution of simulated sea surface temperature was also quite reasonable, without obvious climate drift. FGOALS1.1-s is also capable of capturing the major features of the climatological mean state of the EASM: major rainfall maximum centers, the annual cycle of precipitation, and the lower-level monsoon circulation flow were highly consistent with observations in the EASM region.

Regarding interannual variability, simulation of the EASM leading patterns and their relationship with sea surface temperature was examined. The results show that FGOALS1.1-s can reproduce the first leading pattern of the EASM and its close relationship with the decaying phase of the ENSO. However, the model lacked the ability to capture either the second major mode of the EASM or its relationship with the developing phase of the ENSO.

Key words: East Asian Summer Monsoon, ocean–atmosphere–land model, climatological mean state, interannual variability, ENSO

Citation: Bao, Q., G. X. Wu, Y. M. Liu, J. Yang, Z. Z. Wang, and T. J. Zhou, 2010: An introduction to the coupled model FGOALS1.1-s and its performance in East Asia. *Adv. Atmos. Sci.*, **27**(5), 1131–1142, doi: 10.1007/s00376-010-9177-1.

1. Introduction

The East Asian Summer Monsoon (EASM) influences about one quarter of the world's population. Developing a state-of-the-art climate model to simulate the realistic EASM has therefore become one of the chief concerns for the climate modeling community, but especially in China.

Air–sea coupling is a crucial process in the Asian monsoon regions where the atmospheric feedback on SST is important, and, due to the involvement of air–sea interactions, coupled air–sea models have a better ability to capture a realistic simulation than atmosphere-only models (e.g., Fu and Wang, 2003; Wang et al., 2005a). Through evaluating the simulations of the major modes of the Asian summer mon-

*Corresponding author: BAO Qing, baoqing@mail.iap.ac.cn

soon by the ten fully coupled atmosphere–ocean–land models, Wang et al. (2007) pointed out that models can provide reasonable simulations of the first two leading modes of the Asian monsoon after introducing the air-sea coupling. Therefore, developing a fully coupled climate model has become a necessary step in order to simulate the East Asian monsoon system.

Chinese scientists have been developing Atmospheric General Circulation Models (AGCMs) and Ocean General Circulation Models (OGCMs) since the 1980s. In the early 1990s, scientists in the State Key Laboratory of Numerical Modeling for Atmospheric Sciences and Geophysical Fluid Dynamics at the Institute of Atmospheric Physics (LASG/IAP) began to develop their model. And, at the end of the 20 century, the first generation air–sea coupled model, named GOALS, was released owing to these efforts (Zhang et al., 2000). Indeed, such was its success, that the relevant IPCC version of GOALS participated in the third IPCC coordinated experiments.

In 2004, the first version of the Flexible Global Ocean–Atmosphere–Land System (FGOALS 1.0) model was released by LASG/IAP, and this model has provided state-of-the-art computer simulations of the Earth's past, present, and future climate states (Zhou et al., 2005; Bao et al., 2006; Wang et al., 2007). In terms of the configuration of FGOALS1.0, there are two atmospheric components. The spectral version—the Spectral Atmospheric Model of the IAP and LASG (SAMIL) (Wu et al., 1996; Wu et al., 2004; Wang et al., 2005b; Bao et al., 2006) —and the corresponding coupled version, is named FGOALS-s; and the gridded version, GAMIL (Wang et al., 2004) and FGOALS-g is the relevant coupled version (Yu et al., 2004). The oceanic component is LASG IAP Common Ocean Model (LICOM) (Liu et al., 2004), and the other components, including land surface, ice, and coupler components, are from the NCAR CCSM2 (Kiehl and Gent, 2004). Compared to GOALS, the resolution of each component of FGOALS-s was markedly increased (Liu et al., 2004; Wang et al., 2005b), as well as several of the major physical processes having been improved (Zhou et al., 2005). FGOALS-s also makes full use of advanced computing technologies, including the climate model coupler, application of the Message Passing Interface (MPI), and standard input/output (I/O) with network Common Data Form (NetCDF).

However, FGOALS1.0-s has been shown to possess several biases in its simulations of energy balance at the top of the atmosphere, of land and sea surface temperatures, of cloud amounts, and of rainfall distributions in the Asian monsoon regions (Zhou et al., 2005; Wang et al., 2007). To overcome these biases, it is necessary for the physical processes in SAMIL to be further modified.

This paper will describe some major modifications to the physical parameterization packages in the spectral atmospheric component of FGOALS (FGOALS-s, the new version being called FGOALS1.1-s) and will report on an evaluation of the new model's performance in simulating the East Asian Summer Monsoon mean state and its interannual variability. An introduction to FGOASLS1.1-s and the main modifications made to its component models are described in section 2. The datasets used in the study are introduced in section 3. Section 4 presents and evaluates the results from using the new-coupled model to simulate the EASM. And finally, the last section provides some discussion and conclusions.

2. Models and numerical experiments

2.1 *General description of the model*

There are five active components under the framework of FGOALS1.1-s (FGOAOLS-s in short hereafter). The atmospheric component of FGOALS-s is version 2.2.3 of SAMIL, which was developed at LASG/IAP. It is a spectral transform model with 26 atmospheric layers extending from the surface to 2.19 hPa, and its horizontal resolution is R42 [which approximates to a resolution of about 2.81° (lon)×1.66°(lat)]. The time increment of integration in the current version of SAMIL R42L26 is 10 mins. The radiation scheme is the Edwards-Slingo scheme from the UK Meteorological Office (Edwards and Slingo, 1996), but with a modification by Sun and Rikus (Sun and Rikus, 1999a,b). The time step of the radiation scheme is one hour, meaning the diurnal cycle of solar radiation can be captured. The mass flux cumulus parameterization of Tiedtke (Tiedtke, 1989) is utilized for deep, shallow and midlevel convection, with a modified closure assumption and the formation of organized entrainment and detrainment (Nordeng, 1994; Song, 2005). The PBL part of the model is a higher-order closure scheme that computes the turbulent transfer of momentum, heat, moisture, and cloud water (Brinkop and Roeckner, 1995). The cloud scheme is a diagnostic method based on vertical motion and relative humidity (Liu and Wu, 1997), and the effects of gravity-wave drag are also applied, which depend on wind speed, density, and static stability of the low-level flow (Palmer et al., 1986).

The oceanic component of FGOALS-s is version 1.1 of LICOM, which was also developed at LASG/IAP. It is a grid-point model with 30 oceanic layers and a horizontal resolution of 1°×1°. The time increment of integration in LICOM1.1 is one hour for thermal pro-

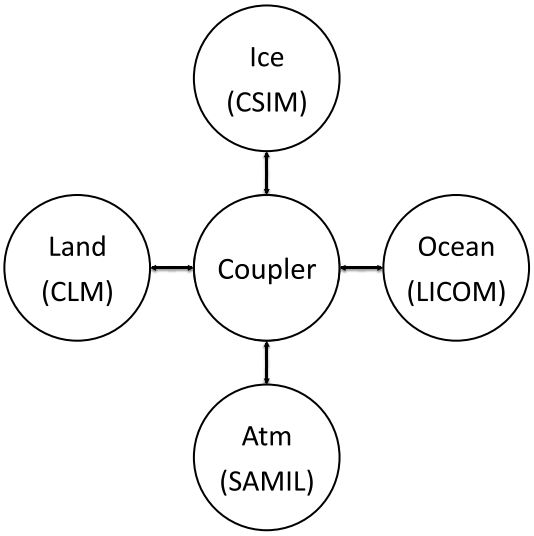

Fig. 1. Schematic diagram of the FGOALS-s1.1 framework.

cesses and three hours for dynamic processes. The land component of the coupled system is the Community Land Model, version 2.0 (CLM2) (Bonan et al., 2002; Bao et al., 2006), and its horizontal resolution is the same as the atmospheric component [about 2.81°(lon)×1.66°(lat)]. Unlike previous land process models (SSiB, Xue et al., 1991; Liu and Wu, 1997), CLM2 can use a flexible time step, which can be different from its atmospheric component. In the present study, 20 mins was used as one time step. The thermodynamic component of the FGOALS-s sea ice model is version 4 of the CCSM sea ice model (CSIM4), which shares the same resolution as LICOM (1°×1°). The coupler used to drive the whole climate system is the NCAR's coupler version 5.0, which was released with CCSM2 and without any flux adjustment. The whole coupled system model is demonstrated in Fig. 1 by a schematic diagram.

2.2 *Modifications to the model*

Compared with the spectral version 1.0 of FGOALS, the improved physical processes in the atmospheric component of FGOALS1.1-s mainly include the Edwards-Slingo radiation parameterization (Edwards and Slingo, 1996), the mass flux cumulus parameterization of Tiedtke (Tiedtke, 1989), and a diagnostic cloud parameterization scheme. In the Edwards-Slingo radiation scheme, the resolution of the shortwave band is extended from four bands to nine, and the longwave band is changed from seven bands to eight. The categories of absorbing air are increased and involve the effects of O_2, CH_4, N_2O and CFCs. Additionally, the direct effects from five kinds of aerosols, including black carbon, brown carbon, sulfate, sea salt and dust (Sun, 2005; Li et al., 2009), are included in the new version of the radiation scheme. The mass flux cumulus parameterization of Tiedtke (Tiedtke, 1989) is switched to the original version of the Tiedtke scheme with the tuning of lateral convective entrainment/detrainment rate for shallow convection, the relative humidity threshold for the triggering of deep convection, and the efficiency for the conversion of cloud water to rainwater (Liu et al., 2007). In the diagnostic cloud scheme, the threshold for low cloud is modified to take account of the differences among land, sea and regions of snow/ice cover.

In addition, the source of coding of SAMIL has been updated with Fortran 90 syntax, and many advanced technologies (including dynamic memory, the use of module and interface syntax etc.) have been adopted to save computing memory as well as speed up the integration.

2.3 *Description of the coupled integration*

FGOALS-s has been integrated for 60 years with the external forcing of the fixed greenhouse gases in 1990. The climatological aerosol distribution is derived from 3D reanalysis datasets, which are generated by the Takemura et al. (2000). The direct effects of the 3D aerosol distributions for five climatological types of aerosol (black carbon, origin carbon, sulfate, sea salt, and dust) are taken into consideration in the coupled integration. These fully coupled system models are driven by the coupler with mode MPMD (Multiple Program Multiple Data Stream Computers). Table 1 presents the time step for each individual component model and their communication frequencies with the coupler. Since the communication frequency is one hour between SAMIL and the coupler, the time step for calculating radiation effects of short and long waves has to be shortened from three hours to one. Owing to the constraint of disk space, only monthly outputs

Table 1. The time steps and communication frequencies with the coupler for each component model in FGOALS-s1.1.

	SAMIL (atm)	LICOM (ocn)	CLM (lnd)	CSIM (ice)
Time step	10 minutes	Barotropic processes: 2 minutes Baroclinic processes: 1 hour Heat and salt: 3 hours	20 minutes	1 hour
Communicating frequency	1 hour	1 day	1 hour	1 hour

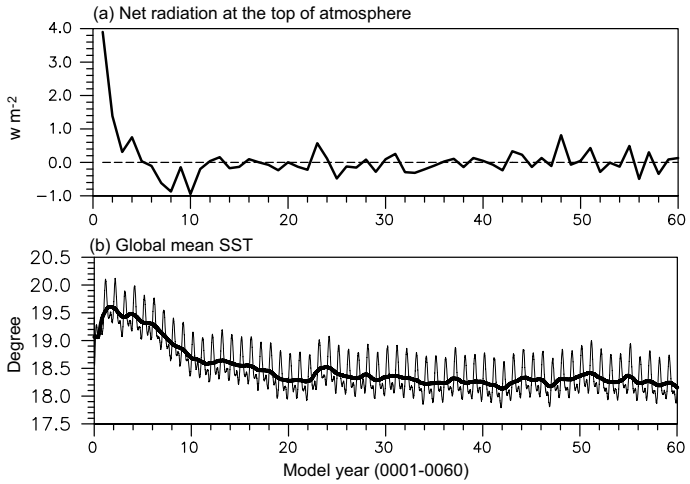

Fig. 2. Time series of the global mean (a) net radiation at the TOA (thick line; W m^{-2}) and (b) SST (thin line; °C). The thick line in (b) represents the 365-day running mean of SST.

from all component models are saved for analysis.

3. Datasets and methodology

The datasets used for evaluating the model include the climatological SST dataset from the UK Meteorological Office's Hadley Centre (HadISST) (Rayner et al., 2003), the NCEP–NCAR reanalysis circulation fields (Kalnay et al., 1996), and precipitation data from the Global Precipitation Climatology Project (GPCP) (Xie et al., 2003). To be consistent with the model, all the datasets were gridded to a resolution of 2.81°(lon) ×1.66° (lat)

To obtain the leading modes of EASM interannual variability, a multivariate EOF analysis (MV-EOF) was applied (Liu et al., 2008). The four variables selected for this analysis include observed precipitation, sea-level pressure, 850 hPa zonal winds, and 850 hPa meridional winds. The MV-EOF analysis method is described in detail in Wang (1992). The method has the advantage of capturing spatial phase relationships among various selected circulation and precipitation fields. In the MV-EOF analysis, an area-weighted, normalized covariance matrix was constructed for the combined four meteorological fields. After the EOF decomposition, dimensional eigenvectors (spatial patterns) were obtained.

4. Results

4.1 *Net radiation at the top of the atmosphere and SST*

The net radiation flux at the top of the atmosphere (TOA) and SST are two crucial measures to reflect climate drift in the complex coupled ocean and atmosphere model system. Figures 2a and 2b show the time series of global mean net radiation flux at the TOA and in SSTs respectively, taken from the free-coupled integration of FGOALS-s over 60 years. The two curves demonstrate that it took about 15 years for the coupled system to reach a stable state; namely, the spin-up process was about 15 years, which is the same as FGOALS-s1.0 (Zhou et al., 2005). The excessive net radiation at the TOA during the first 15 years resulted in a positive global mean SST anomaly during the spin-up process. As the net radiation at the TOA became more balanced, the global mean SST also reached a steady state. The averaged global mean net radiation flux shows that FGOALS-s successfully achieved energy balance at the TOA, and the 40-year climatological mean (from 0021 to 0060 in model years) was 0.003 W m^{-2}. At the same time, as shown in Fig. 2b, there was no remarkable climate drift in the coupled integration, as demonstrated from the global mean SST.

Figure 3 shows simulated and observed SST distributions for the annual mean (upper panel of Fig. 3), summer mean [June, July, August (JJA); lower panel of Fig. 3], and winter mean (December, January, February (DJF); middle panel of Fig. 3). The mean SST in the model was derived from the 0041 to 0060 integrated years.

Generally speaking, no remarkable climate drift of SST could be detected, either in the annual mean or seasonal mean. Previous studies have documented that the double ITCZ is a modeling bias, which frequently appears in many models (e.g. Mechoso et al., 1995), often referred to as the coupled GCM "double ITCZ syndrome" (Ma et al., 1996). However, accord-

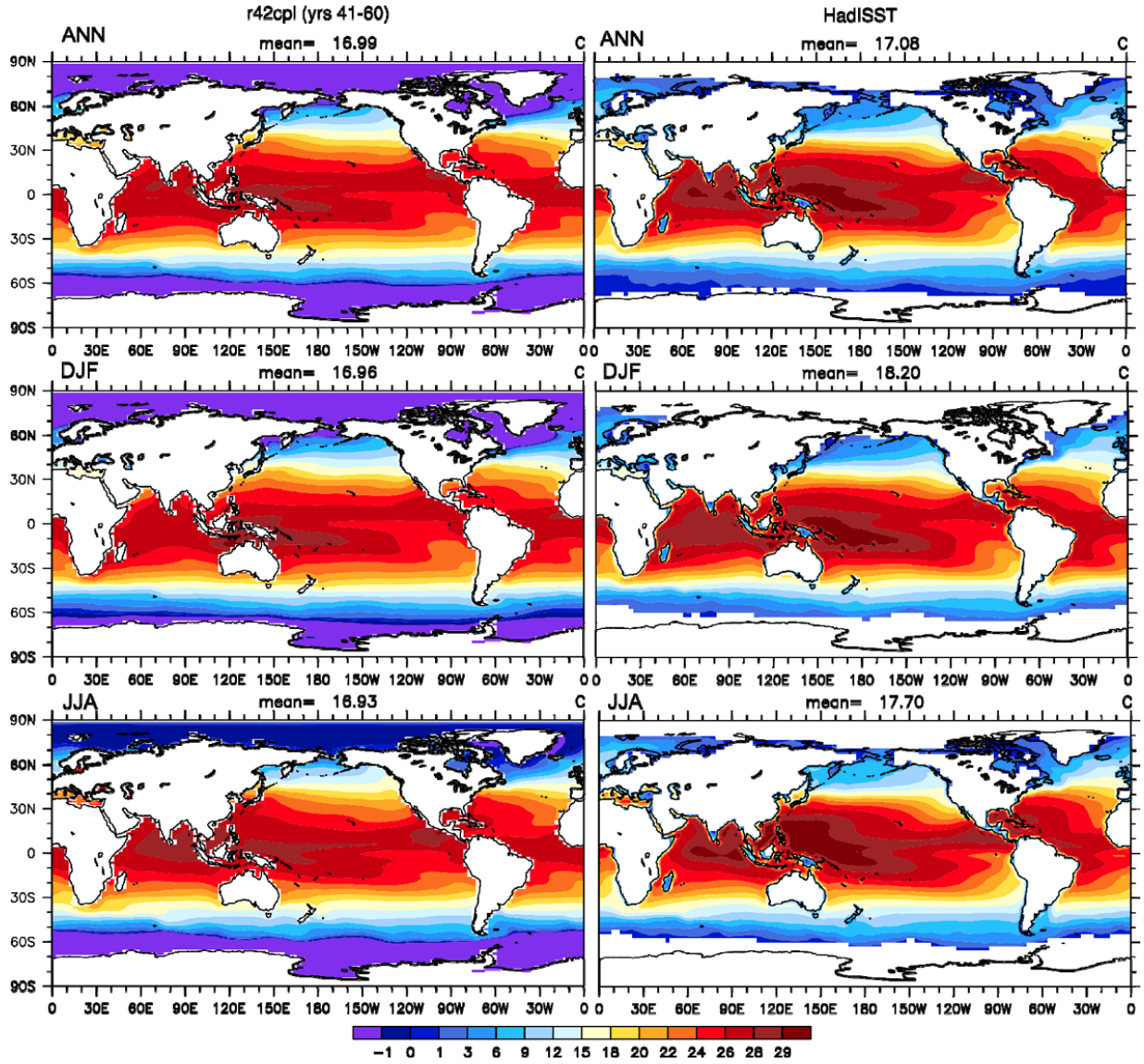

Fig. 3. The distributions of simulated (left panels) and observed (right panels) SST (°C) in the annual mean (ANN), winter time (DJF) and summer time (JJA).

ing to the results from both SST and precipitation (figure not shown), the double ITCZ did not appear in the results of FGOALS1.1-s, which might have been due to the benefit of the special low cloud scheme. This scheme is based on a statistical method related to lower-level stability (Dai et al., 2005), thereby enabling the model to reasonably catch two low cloud centers: one along the west coast of North America, and the other west of the coast of Peru.

The major differences between the coupled model and observations come from the warm pool regions. The model underestimated the maximum SST by around one degree, and consequently the meridional SST gradient between the tropics and extratropics was too small. The negative meridional SST gradient may have weakened the heat transport from the equatorial regions to the higher latitude regions, and this bias has also been found in the previous version of FGOALS-s (Zhou et al., 2005). Two reasons are assumed for this bias. One derives from the fact that simulated convection in the warm pool regions tends to be too strong, which blocks downward solar radiation and generates too much surface evaporation, cooling the underlying sea surface. The other reason arises from ocean vertical mixing being too strong in this region. Regarding the overestimation of convection, this may be attributable to atmospheric convection occurring too easily, or to feedback between convection and circula-

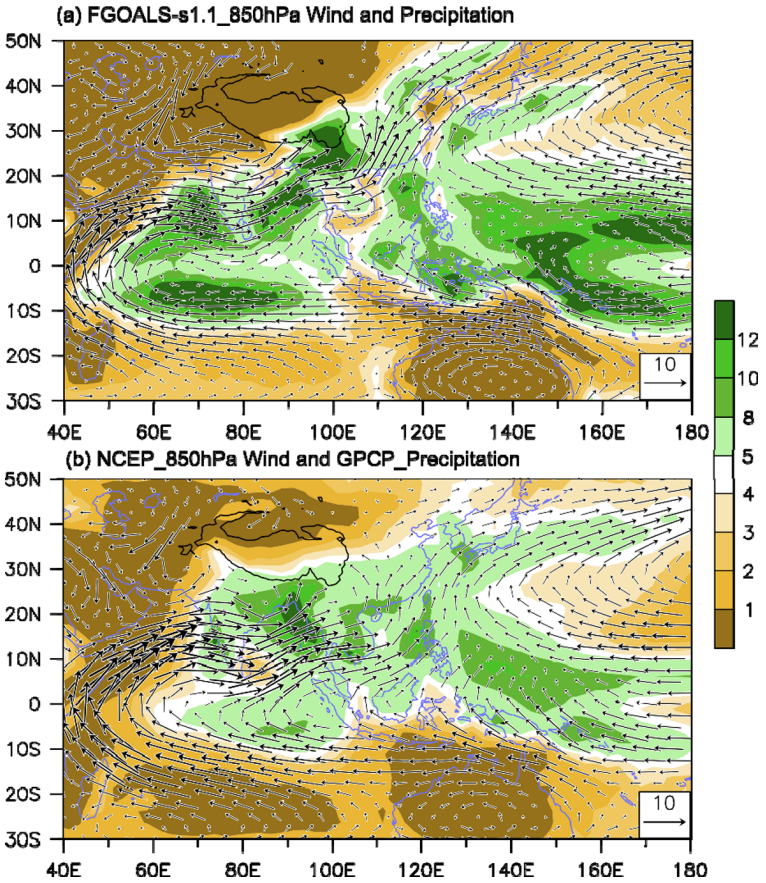

Fig. 4. Climatological summer (JJA) mean precipitation (colored shading in mm d^{-1}) and 850 hPa winds (vectors in units of m s^{-1}) in (a) FGOALS-s1.1 and (b) observed results (wind data are from the NCEP reanalysis dataset and precipitation from the GPCP dataset).

tion being too strong. Therefore, retuning the atmospheric cumulus parameterization scheme may help to solve the warm-pool cold bias.

4.2 *The climatological EASM*

The lower level wind (850 hPa) and rainfall in both FGOALS1.1-s and observations are presented in Fig. 4. Over the Indian Ocean region, the model was able to reproduce South Asian monsoon circulation, including the cross-equatorial low-level jet (namely the Somali Jet), and two monsoon troughs: one located to the east of the Arabian Peninsula and the other over the South China Sea. Associated with the Somali Jet and the two monsoon troughs, there were three distinguished monsoon rainfall centers: the first along the western coast of the Arabian Peninsula, the second over the Bay of the Bengal, and the third over the South China Sea. Compared with GPCP observations, the locations of these three monsoon rainfall centers were simulated well, although the rainfall intensity was slightly overestimated in the results of FGOALS-s1.1. Over the Western Pacific regions, the Western North Pacific (WNP) Subtropical High (SH) (WNPSH) dominated the circulation system. FGOALS-s showed a remarkable ability to reproduce this climatological WNP subtropical anticyclone, and the simulated ridgeline of the WNP subtropical anticyclone was around 24°N, consistent with observations. Along the northern flank of the WPSH was the East Asian subtropical rain belt. As illustrated in Fig. 4, the model simulated this southwest–northeast tilted rainfall belt.

The annual cycle of rainfall over the EA region (averaged from 110°E to 120°E) can be examined by the simulation results shown in Fig. 5, which illustrates the seasonal march and retreat of EA rainfall. Compared with the rainfall march derived from GPCP data, FGOALS-s captured reasonably the dry and wet phases of the East Asian monsoon. The clearly persistent rainfall beginning in the middle of February [namely the EA spring persistent rainfall (Wu et al., 2007)] is visible in the model's results, and the northward march of the monsoon rainfall was also reproduced well with the movement of the solar position, both of which are consist with observations. Regard-

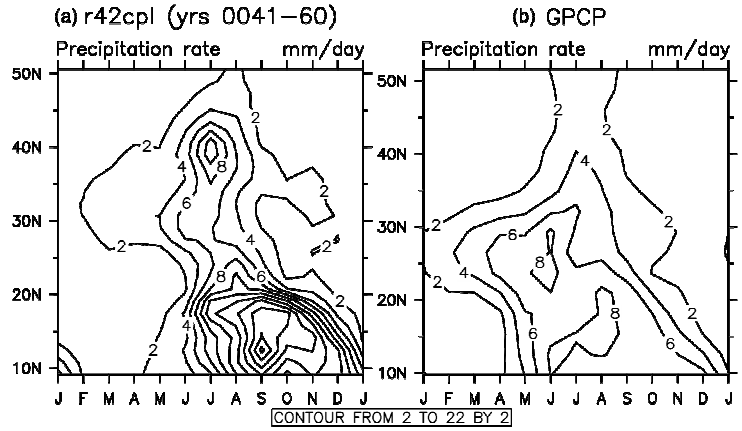

Fig. 5. Climatological annual cycle of 110°–120°E zonal mean precipitation (mm d^{-1}) in (a) FGOALS-s1.1 and (b) GPCP. The contours are from 2 to 22 with an interval of 2.

ing the retreat of EA rainfall, FGOALS-s1.1 also simulated well the major features of this process, which was characterized by slow and smooth trends.

Overall, FGOALS-s has shown a strong ability to simulate the climatological mean of the EASM, and simulations of the main rainfall centers, the seasonal march and retreat of precipitation, and the lower level monsoon flow, were all consistent with observations in the EASM region.

4.3 *Leading patterns of EASM interannual variability and its relationship with SST*

Through MV-EOF analysis, Wang et al. (2008) pointed out that the leading patterns of EASM interannual variability are dominated by variations of the WNPSH. As illustrated in Figs. 6a and 7a, the observed first leading pattern accounted for 38% of the total variation in interannual variability, and the corresponding distributions of dry and wet phases were closely related with the southwest extension of the WNPSH. The subtropical rainfall belt was located to the north of the WNPSH and the negative rainfall belt was under the control of the WNPSH. Figures 6b and 7b show the second leading pattern of the EASM and its corresponding principal component, which carried 11.3% of the total variation. Furthermore, the spatial pattern of the second mode indicates a weakening of the EASM, which was characterized by a weakened WNPSH and the southward retreat of the WNP monsoon trough. The seasonal evolution of SST anomalies associated with the two leading modes are shown in Fig. 8, which indicates that the observed first leading mode of EASM interannual variability was significantly related to a decaying phase of El Niño, while the second mode was closely related to the developing phase of El Niño.

The question, then, is how well can FGOALS1.1-s capture the leading patterns of the EASM? Figures 6c and 7c show the two simulated leading patterns and their corresponding principal components, of the EASM, which were derived from the last 27 model years. The first leading mode accounted for approximately 38% of the total variation of EASM interannual variability, which is exactly the same as was observed. The first leading mode of the simulated EASM was also characterized by a prominent abnormal WNPSH, which again is very close to what was observed. Meanwhile, as shown in Fig. 9a, the regressed seasonal evolution of SST anomalies suggests that the first leading mode was related to the decaying phase of El Niño. However, as shown in Figs. 6d and 9b, FGOALS1.1-s could not capture the same second leading pattern of EASM interannual variability and its relationship with the developing phase of El Niño. Regarding this, Zhou et al. (2009) proposed that most of the IPCC's AR4 models also fail to identify the second major mode, and thus more studies are needed to investigate the cause of this problem.

5. Discussion and conclusions

In order to develop a state-of-the-art fully coupled climate model and obtain realistic simulations of the EASM, the radiation cloud scheme and cumulus convection parameterization of SAMIL have been updated in a new generation FGOALS-s model (version 1.1 of FGOALS-s). The behavior of the simulated EASM in FGOALS1.1-s has been presented from three aspects:

(1) Performance of the simulated energy balance at the TOA and in SSTs. These can be considered as the important indices to exhibit the stability of the whole coupled climate system and the results suggest that FGOALS1.1-s can successfully achieve the energy balance at the TOA. Additionally, there was no signif-

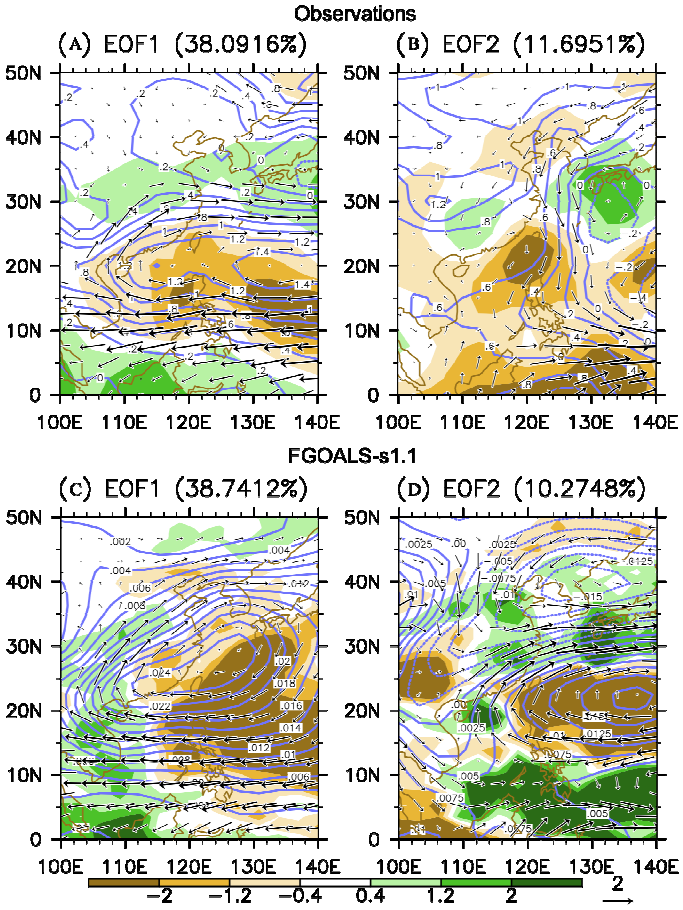

Fig. 6. Observed (a and b) and simulated (c and d) spatial patterns of the first two MV-EOF modes of the EASM. Shown in the panels are 850 hPa winds (vectors in units of m s^{-1}), precipitation (colored shading in units of mm d^{-1}), and sea-level pressure (contours in units of hPa).

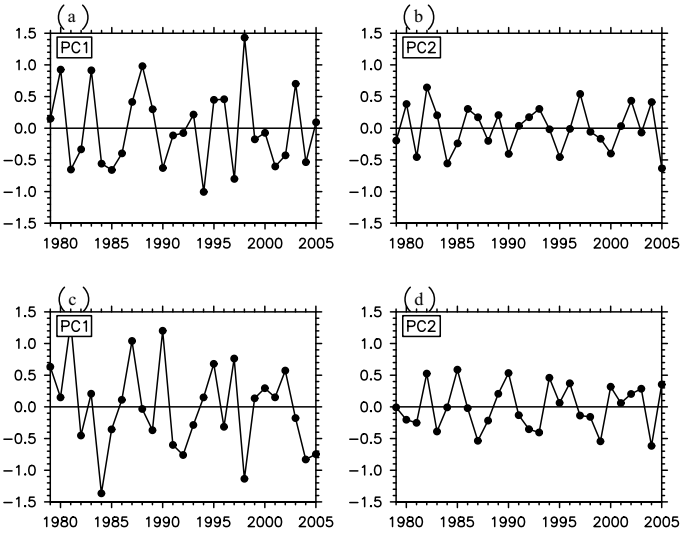

Fig. 7. Observed (a and b) and simulated (c and d) corresponding principal components of the first two MV-EOF modes of the EASM.

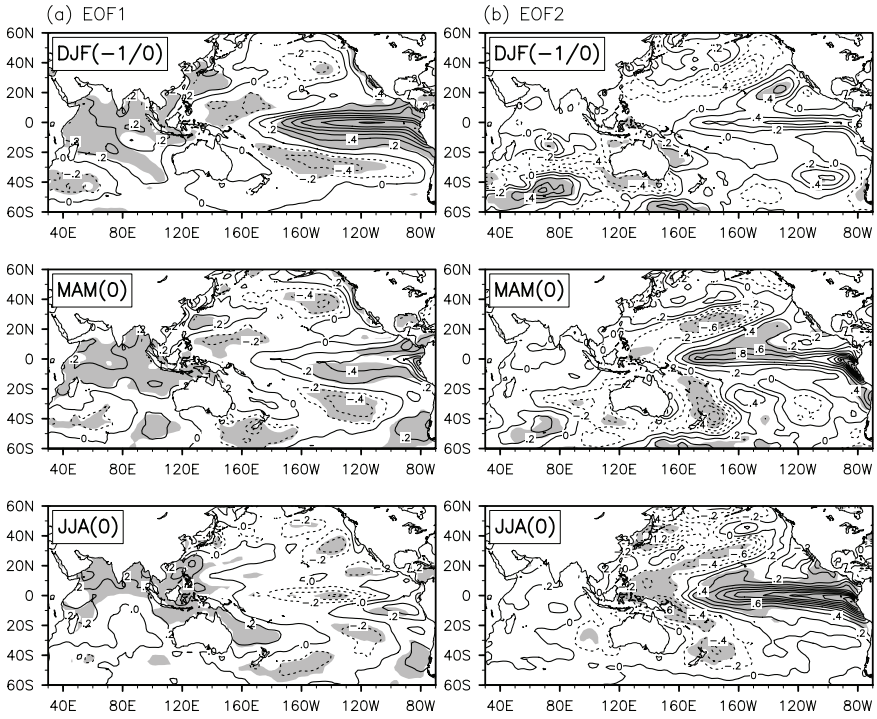

Fig. 8. Evolution of SST anomalies associated with the two MV-EOF modes (°C). Patterns were obtained by regressing with respect to the first two principal components of the MV-EOF analysis for three consecutive seasons: DJF(−1/0), MAM(0), and JJA(0), where "0" denotes the year concurring with the EA-WNP leading modes. "−1" denotes the year preceding year 0. Grey shading indicates areas where the anomalies are statistically significant at the 5% level.

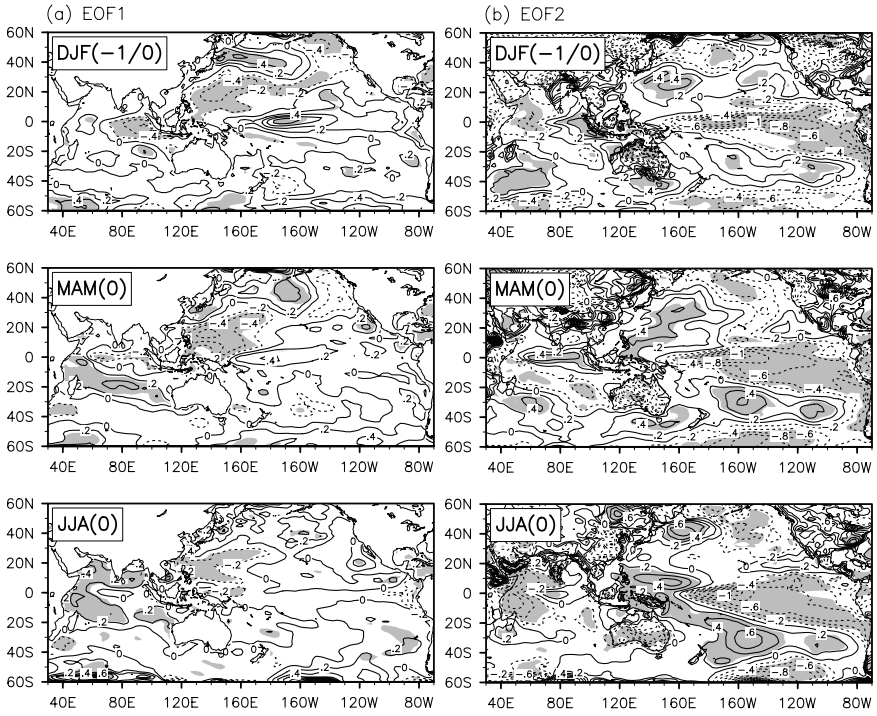

Fig. 9. As in Fig. 8 but for FGOALS-s1.1.

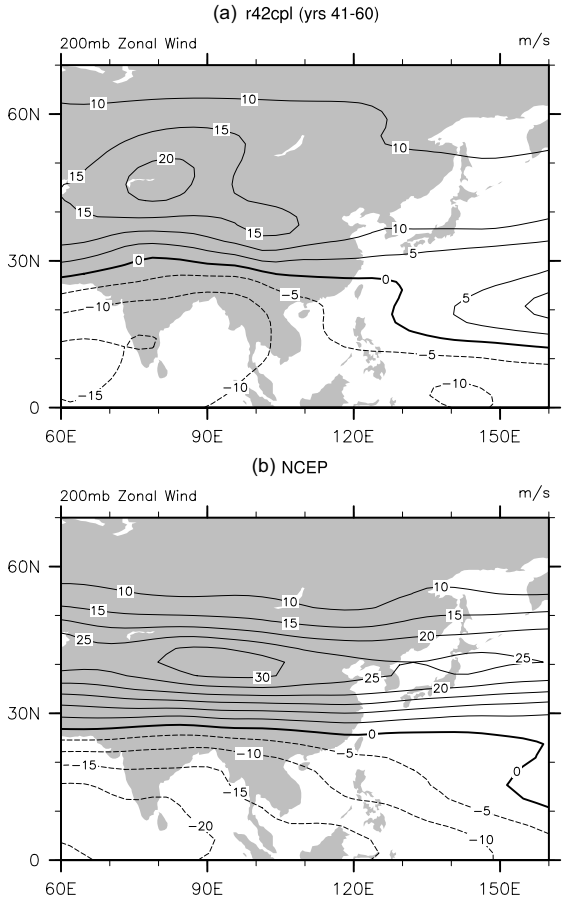

Fig. 10. Climatological summer (JJA) mean 200 hPa zonal winds (contours in units of m s^{-1}) in (a) FGOALS-s1.1 and (b) NCEP reanalysis data.

icant climate drift detected in this study.

(2) Behavior of the mean EASM. It has been demonstrated that the model has remarkable ability to simulate the climatological lower level monsoon jet flow and monsoon rainfall. Meanwhile, the simulated seasonal advance and retreat of the rainy season over the EA was also comparable to observations.

(3) Behavior of EASM interannual variability. The results show that the model can capture the first leading pattern of EASM interannual variability and its relationship with the decaying phase of El Niño, but fails to reproduce the second major mode of the EASM and its relationship with the developing phase of El Niño.

Compared to the previous version of FGOALS1.0-s, the major improvements of FGOALS1.1-s come from the simulated distribution of the tropical SST. As shown in Zhou et al. (2005; Figure 5.3.2), the cold tongue extended westward too much in FGOALS1.0-s, but this problem has been much improved in FGOALS1.1-s (Fig. 3). In addition, in both the Indian Ocean and Western Pacific Ocean, simulated tropical SST in FGOALS1.1-s was more realistic than in FGOALS1.0-s.

Nevertheless, there are still several unsolved problems with FGOALS1.1-s relating to the EASM. For example, the EA upper-level jet flow is one of the important indices for gauging the simulation of the EASM. Guo et al. (2008) found that the simulated upper-level jet flow was quite weak when using the previous version of FGOALS-s (version 1.0). Figure 10 shows the zonal wind at 200 hPa in the current version of the coupled model, along with NCEP reanalysis data. Compared with results from the previous version of FGOALS-s, there was no notable improvement in terms of the simulation of this upper level jet flow. The reason for the bias may come from the unrealistic 3D distribution of the temperature in the simulation. There was a cold bias of temperature in the upper levels over the Tibetan Plateau. Further analysis suggests that the abnormal negative latent heating release from the cumulus convective processes should have contributed to this upper-level cold bias, since there was a dry bias (Fig. 4a) over the Tibetan Plateau. Accordingly, a retuning of the cumulus scheme is necessary so that this problem can be resolved.

Regarding the simulated interannual variability, it has been shown that the major modes of EASM interannual variability are primarily associated with the ENSO (Wang et al., 2008; Liu et al., 2008). Consequently, the simulated evaluation of the ENSO in the current model can be helpful to understand why the coupled model cannot reasonably present the major modes of the EASM and their relationship with SST anomalies. This work will be reported in a later paper.

Acknowledgements. The authors would like to thank the two anonymous reviewers for their valuable suggestions. This research was jointly supported by the National Natural Science Foundation of China (40890054, 40805038), the 973 Program of China (2010CB950404), the R&D Special Fund for Public Welfare Industry (meteorology) (GYHY200806006), the Chinese Academy of Sciences (KZCX2-YW-Q11-04), and the National Science & Technology Pillar Program of China (2007BAC29B03).

REFERENCES

Bao, Q., Y. Liu, T. Zhou, Z. Wang, G. Wu, and P. Wang, 2006: The sensitivity of the Spectral Atmospheric General Circulation Model of LASG/IAP to the land process. *Chinese J. Atmos. Sci.*, **30**, 1077–1090. (in Chinese)

Bonan, G. B., K. W. Oleson, M. Vertenstein, and S. Levis,

2002: The land surface climatology of the Community Land Model coupled to the NCAR Community Climate Model. *J. Climate*, **15**, 3123–3149.

Brinkop, S., and E. Roeckner, 1995: Sensitivity of a general-circulation model to parameterizations of cloud-turbulence interactions in the atmospheric boundary-layer. *Tellus* (*A*), **47**, 197–220.

Dai, F., R. Yu, X. Zhang, and Y. Yu, 2005: A statistical low-level cloud scheme and its tentative application in a general circulation model. *Acta Meteorologica Sinica,* **19**, 263–274.

Edwards, J. M., and A. Slingo, 1996: A studies with a flexible new radiation code. I: Choosing a configuration for a large-scale model. *Quart. J. Roy. Meteor. Soc*, **122**, 689–720.

Fu, X. H., and B. Wang, 2003: Influences of continental monsoons and air–sea coupling on the climate of the equatorial Pacific. *J. Climate*, **16**, 3132–3152.

Guo, L. L., Y. Zhang, B. Wang, L. Li, T. Zhou, and Q. Bao, 2008: Simulations of the East Asian Subtropical Westerly Jet by LASG/IAP AGCMs. *Adv. Atmos. Sci.*, **25**(3), 447–457.

Kalnay, E., and Coauthors, 1996: The NCEP/NCAR 40-year reanalysis project. *Bull. Amer. Meteor. Soc.*, **77**, 437–471.

Kiehl, J. T., and P. R. Gent, 2004: The Community Climate System Model, Version 2. *J. Climate*, **17**, 3666–3682.

Li, J., Y. Liu, Z. Sun and G. Wu, 2009: The impacts of the radiation and cumulus convective parameterization on the radiation fluxes in SAMIL. *Acta Meteorologica Sinica*, **67**(3), 355–36. (in Chinese)

Liu, H., and G. X. Wu, 1997: Impacts of land surface on climate of July and onset of summer monsoon: A study with an AGCM plus SSiB. *Adv. Atmos. Sci.*, **14**, 289–308.

Liu, H. L., X. Zhang, W. Li, Y. Yu, and R. Yu, 2004: An eddy-permitting oceanic general circulation model and its preliminary evaluations. *Adv. Atmos. Sci.*, **21**, 675–690.

Liu, J., B. Wang, and J. Yang, 2008: Forced and internal modes of variability of the East Asian summer monsoon. *Climate of the Past*, **4**, 645–666.

Liu, Y., K. Liu, and G. X. Wu, 2007: The impacts of the cumulus convective parameterization on the atmospheric water-content and rainfall simulation in SAMIL. *Chinese J. Atmos. Sci.*, **31**(6), 1201–1211. (in Chinese)

Ma, C. C., C. R. Mechoso, A. W. Robertson, and A. Arakawa, 1996: Peruvian stratus clouds and the tropical Pacific circulation: A coupled ocean–atmosphere GCM study. *J. Climate*, **9**, 1635–1645.

Mechoso, C. R., and Coauthors, 1995: The seasonal cycle over the tropical Pacific in coupled ocean–atmosphere general circulation models. *Mon. Wea. Rev.*, **123**, 2825–2838.

Nordeng, T. E., 1994: Extended versions of the convective parameterization scheme at ECMWF and their impact on the mean and transient activity of the model in the tropics. *ECMWF Technical Memo.* 206, Reading, England, 41pp.

Palmer, T. N., G. J. Shutts, and R. Swinbank, 1986: Alleviation of a systematic westerly bias in general circulation and numerical weather prediction models through an orographic gravity wave drag parameterization. *Quart. J. Roy. Meteor. Soc.*, **112**, 1001–1039.

Rayner, N. A., D. E. Parker, E. B. Horton, C. K. Folland, L. V. Alexander, D. P. Rowell, E. C. Kent, and A. Kaplan, 2003: Global analyses of sea surface temperature, sea ice, and night marine air temperature since the late nineteenth century. *J. Geophys. Res.*, **108**(D14), 4407–4436.

Song, X. L., 2005: The evaluation analysis of two kinds of mass flux cumulus parameterizations in climate simulation. Ph. D. dissertation, Institute of Atmospheric Physics, Chinese Academy of Sciences, 119–145. (in Chinese)

Sun, Z., 2005: Parameterizations of radiation and cloud optical properties. BMRC Research Report, 107–112.

Sun, Z., and L. Rikus, 1999a: Improved application of ESFT to inhomogeneous atmosphere. *J. Geophys. Res.*, **104**, 6291–6303.

Sun, Z., and L. Rikus, 1999b: Parameterization of effective radius of cirrus clouds and its verification against observations. *Quart. J. Roy. Meteor. Soc.*, **125**, 3037–3056.

Takemura, T., H. Okamoto, Y. Maruyama, A. Numaguti, A. Higurashi, and T. Nakajima, 2000: Global three-dimensional simulation of aerosol optical thickness distribution of various origins. *J. Geophys. Res.*, **105**, 17853–17873.

Tiedtke, M., 1989: A comprehensive mass flux scheme for cumulus parameterization in large-scale models. *Mon. Wea. Rev.*, **117**, 1779–1800.

Wang, B., 1992: The vertical structure and development of the ENSO anomaly mode during 1979–1989. *J. Atmos. Sci.*, **49**(8), 698–712.

Wang, B., H. Wan, and Z. Ji, 2004: Design of a new dynamical core for global atmospheric models based on some efficient numerical methods. *Science in China* (*A*), **47**, 4–21.

Wang, B., and Coauthors, 2005a: Fundamental challenge in simulation and prediction of summer monsoon rainfall. *Geophys. Res. Letts.*, **32**, L15711.

Wang, B., and Coauthors, 2008: How accurately do coupled climate models predict the Asian-Australian monsoon interannual variability? *Climate Dyn.*, **30**, 605–619.

Wang, Z., G. Wu, and P. Liu, 2005b: The development of GOALS/LASG AGCM and its global climatological features in climate simulation. I—Influence of horizontal resolution. *Journal of Tropical Meteorology*, **21**, 225–237. (in Chinese)

Wang, Z., R. Yu, Q. Bao, T. Zhou, Y. Liu, P. Wang, and G. Wu, 2007: A comparison of the atmospheric circulations simulated by the FGOALS-s and SAMIL. *Chinese J. Atmos. Sci.*, **31**, 202–213. (in Chinese)

Wu, T., Z. Wang, Y. Liu, R. Yu, and G. Wu, 2004: An

evaluation of the effects of cloud parameterization in the R42L9 GCM. *Adv. Atmos. Sci.*, **21**, 153–162.

Wu, G., H. Liu, Y. Zhao, and W. Li, 1996: A nine-layer atmospheric general circulation model and its performance. *Adv. Atmos. Sci.*, **13**(1), 1–18.

Wu, G., and Coauthors, 2007: The influence of mechanical and thermal forcing by the Tibetan Plateau on Asian climate. *J. Hydrometeor*, **8**, 770–789.

Xie, P. P., and Coauthors, 2003: GPCP pentad precipitation analyses: An experimental dataset based on gauge observations and satellite estimates. *J. Climate*, **16**, 2197–2214.

Xue, Y. K., P. J. Sellers, J. L. Kinter, and J. Shukla, 1991: A simplified biosphere model for global climate studies. *J. Climate*, **4**, 345–364.

Yu, Y., X. Zhang, and Y. Guo, 2004: Global coupled ocean–atmosphere general circulation models in LASG/IAP. *Adv. Atmos. Sci.*, **21**, 444–455.

Zhang, X., G. Shi, H. Liu, and Y. Yu, 2000: *IAP Global Ocean-Atmosphere-Land System Model*. Beijing, Science Press, 252pp.

Zhou, T., Y. Yu, Z. Wang, and T. Wu, 2005: *Impacts of Ocean–Land–Atmosphere Interactions over the East Asian Monsoon Region on the Climate in China*. Vol. 4, *Atmospheric Circulation Global Model* (*SAMIL*) *and the Coupled Model* (*FGOALS-s*), Beijing, China Meteorological Press, 288pp. (in Chinese)

Zhou, T., B. Wu, and B. Wang, 2009: How well do atmospheric general circulation models capture the leading modes of the interannual variability of the Asian–Australian Monsoon? *J. Climate*, **22**, 1159–1173.